Ferromagnetic resonance in epitaxial $(In_{0.53}Ga_{0.47})_{1-x}Mn_xAs$: Angle- and temperature-dependent studies

K. Dziatkowski,[1,*] M. Palczewska,[2] T. Słupiński,[1] and A. Twardowski[1]
[1]*Institute of Experimental Physics, Warsaw University, Hoża 69, 00-681 Warsaw, Poland*
[2]*Institute of Electronic Materials Technology, Wólczyńska 133, 01-919 Warsaw, Poland*
(Received 22 December 2003; revised manuscript received 7 April 2004; published 7 September 2004)

Ferromagnetic resonance was investigated in MBE grown InGaMnAs epilayers. Strong azimuthal (in-plane) and polar (out-of-plane) anisotropy was observed, and described reasonably with Magnetic-Anisotropy-Energy (MAE) model taking into account both magnetocrystalline and demagnetization contributions. The different symmetries of mixed (cubic+uniaxial) anisotropy revealed by nominally the same epilayers were successfully interpreted in terms of MAE model parameters. This difference was attributed to the possible different ordering in distribution of magnetic ions, originating from subtle changes of the growth process.

DOI: 10.1103/PhysRevB.70.115202 PACS number(s): 75.50.Pp, 76.50.+g, 75.30.Gw, 75.70.Ak

I. INTRODUCTION

Ferromagnetic resonance (FMR) is known to be a powerful mean to study details of magnetic properties of ferromagnets, in particular the magnetic anisotropy.[1] Although FMR was mostly used for metallic systems, it was also applied for semiconductors. In the past few years there were several attempts to measure FMR for magnetic semiconductors based on III-V compounds (GaMnAs, InMnAs). These materials attract nowadays considerable attention as they exhibit ferromagnetism with T_C far above 100 K retaining good semiconducting properties, which makes them potentially important for spintronics.[2,3] For a long time electron spin resonance (ESR) investigations were limited to very dilute $Ga_{1-x}Mn_xAs$ and $In_{1-x}Mn_xAs$ ($x \leqslant 0.01$), as only in such a case clear and understandable results were obtained.[4,5] Such dilute systems are paramagnetic in a standard temperature range (above 2 K). On the other hand ESR experiments performed for ferromagnetic $Ga_{1-x}Mn_xAs$ or $In_{1-x}Mn_xAs$ (typically $x > 0.03$) were giving complicated and sample-dependent results. Only very recently GaMnAs growth technology was refined enough to result in high quality ferromagnetic samples, for which FMR could be studied. Clear results were obtained[6] and consistently interpreted using Magnetic-Anisotropy-Energy (MAE) model of FMR,[1] originally applied for metallic systems. One of the most interesting results was pronounced specific magnetic anisotropy of GaMnAs films, which was attributed to the lattice mismatch induced tetragonal distortion present in GaMnAs epilayers grown on GaAs or InGaAs substrates.[6]

In order to verify the hypothesis on the dominating role of the lattice mismatch induced strain for the features of magnetic anisotropy and widen the available data, we performed similar measurements of FMR to that reported in Ref. 6, but for a different ferromagnetic semiconductor, namely $(In_{0.53}Ga_{0.47})_{1-x}Mn_xAs$ deposited (with $In_{0.53}Ga_{0.47}As$ buffer layer) on the InP(001) substrate. The specific composition of the magnetic alloy and the buffer, i.e., the In/Ga ratio, was chosen with the purpose of matching lattice constants of epilayers and the substrate. Our results suggest that the anisotropy observed in InGaMnAs depends significantly also on details of ferromagnetic layer growth conditions, and so on the features of structural disorder in the ultra-highly doped semiconductor.

The paper is organized as follows. We start with the presentation of experimental details, which is followed by FMR results. Then we recall the idea of MAE model, in our work applied to the general case of any direction of the magnetic field and the magnetization. Theoretical considerations include Zener's analysis of the temperature-dependent behavior of FMR.[7] Next we present the discussion, where the data are analyzed with the use of the MAE model. We end up with the conclusions.

II. EXPERIMENTAL

Ferromagnetic III-V semiconductors are prepared as strained thin films deposited nearly lattice-matched on single crystal substrates.[8] The two model semiconductors in this group are $Ga_{1-x}Mn_xAs$ grown on a GaAs(001) substrate and the one with a larger lattice parameter, $In_{1-x}Mn_xAs$, grown on a thick relaxed buffer made of AlGaSb alloy grown on a GaAs(001) substrate. In this paper, we studied an alloy of both GaMnAs and InMnAs, namely $(In_{0.53}Ga_{0.47})_{1-x}Mn_xAs$, with In/Ga composition satisfying the condition of the lattice match to InP(001). The properties of the prototype nonmagnetic semiconductor, $In_{0.53}Ga_{0.47}As/InP(001)$, were investigated with x-ray and transport techniques, and revealed a high crystalline quality of epilayers grown by molecular beam epitaxy (MBE) at the substrate temperatures T_s down to 125°C.[9] The excess arsenic content with respect to the equilibrium content of high temperature grown $In_{0.53}Ga_{0.47}As$, decreases rapidly with rising T_s, and around 200°C (which is the range of our interest) is less than 0.5%. An addition of Mn to $In_{0.53}Ga_{0.47}As$ even in a large excess over an equilibrium Mn solubility (which is in the range 10^{17} cm^{-3}), preserves the regular crystal structure (zinc blende) of InGaMnAs, providing the substrate temperature during the growth was low enough. The growth procedure and the properties of these materials are presented in Refs. 10 and 11. The regular lattice structure of

$(In_{0.53}Ga_{0.47})_{1-x}Mn_xAs$ layers was inspected during MBE growth using reflection high-energy electron diffraction (RHEED). Resulting thin films of a ferromagnetic semiconductor are strained (tetragonally distorted). In the case of $Ga_{1-x}Mn_xAs$, studied in detail by x-ray diffraction (for a review see Ref. 8), Mn increases the lattice parameter causing that the magnetic layer is under compressive strain in the sample plane. In $In_{1-x}Mn_xAs$, the addition of Mn yields a tensile strain, which is thought to be the reason of the magnetization easy-axis to be perpendicular to the sample plane, contrary to the in-plane easy-axis in $Ga_{1-x}Mn_xAs$.

For the measurement presented here, we used two samples from a set grown with constant Mn composition and prepared by MBE at nominally the same conditions. We had chosen these two, since their magnetic properties (e.g., anisotropy) were different, in spite of similar growth parameters like the In/Ga ratio, growth-rate and temperature during the growth, thickness of ferromagnetic layer, composition and structure of the buffer layer. This choice of samples demonstrates that essential ferromagnetic properties in $(In_{0.53}Ga_{0.47})_{1-x}Mn_xAs$ thin films are sensitive to very subtle changes of growth parameters. Samples consisted of 100 nm $In_{0.53}Ga_{0.47}As$ buffer layer deposited on semi-insulating InP(001) substrates, and followed by a 50 nm layer of ferromagnetic semiconductor $(In_{0.53}Ga_{0.47})_{1-x}Mn_xAs$. Manganese composition was fixed at $x=0.13$ in all samples in this series, and the calibration of Mn was based on measurements of the deposition rate of MnAs layer in a separate MBE process. The buffer layer was grown at a high substrate temperature ($T_s=460\,^\circ$C). After the growth of the buffer, the substrate temperature was lowered to $T_s=205\,^\circ$C to enable high Mn contents in an $(In_{0.53}Ga_{0.47})_{1-x}Mn_xAs$ thin film. The substrate temperature was precisely controlled with an infrared thermometer to within a $6\,^\circ$C range during the growth of the ferromagnetic layer in all samples. The arsenic to metals molar ratio was kept relatively low to prevent the excessive incorporation of As since, in our experience, excess As is undesirable for ferromagnetic properties (or rather does not influence ferromagnetism more significantly than the substrate temperature does, contrary to early published results). The two samples studied (denoted here as K322 and K342f2) had the same growth conditions to within a $6\,^\circ$C range of the substrate temperature and within the accuracy of Mn calibration achievable in a standard solid-source MBE machine, which we may assume to be better than about 5 per cent of the actual value. The choice of several parameters during the growth is mutually dependent (e.g., the Mn composition, growth rate, substrate temperature), therefore experimental errors in technological parameters cause the differences in magnetic properties of samples reported below, as well as in structural properties of metastable InGaMnAs. Although both ferromagnetic layers were deposited lattice-matched, some compressive strain was still present. This strain originated in an expansion of InGaMnAs lattice with the addition of Mn, like in the similar case of GaMnAs/GaAs. While the lattice parameter of InGaMnAs versus Mn composition is not calibrated precisely so far, it is hard to estimate the magnitude of this strain. Samples have not been annealed thermally after the MBE growth.

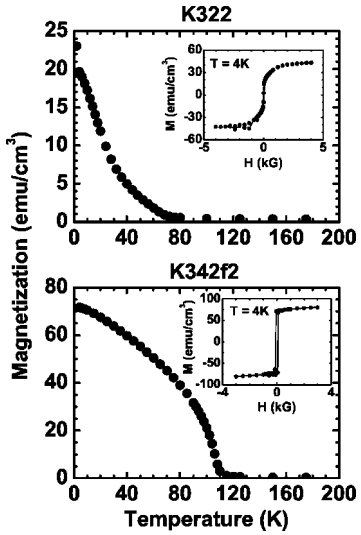

FIG. 1. Temperature-dependent magnetization data of investigated samples with corresponding hysteresis loops (insets).

The samples were characterized by magnetization measurements (Fig. 1). Ferromagnetic behavior was observed for both samples with Curie temperature $T_C=70$ K for K322 and $T_C=110$ K for K342f2, being among the highest values of T_C in InGaMnAs deposited on InP substrates reported so far in the literature.[10,11] In K342f2 most (about 70%) of Mn chemically present in the layer takes part in the ferromagnetic order, while in the other sample, K322, only ~30% of manganese contribute to measured ferromagnetism, as deduced from SQIUD magnetometer data at moderate field $B=3$ T, assuming the magnetic moment of Mn impurity of $\frac{5}{2}\mu_B$.[12] We note that both samples were nominally the same, thus one can expect the same magnetic behavior. This is however not the case. The sample K342f2 exhibited a rectangular hysteresis loop, while K322 showed a rounded very narrow loop with the coercive field of a few Gauss.

In order to study ferromagnetic resonance we used a standard ESR spectrometer working at X-band microwave frequency (~9 GHz), equipped with a continuous-flow helium cryostat. Low-temperature measurements were carried out at about 6 K, however several temperature-dependent investigations were performed as well. The samples were mounted in two positions (Fig. 2): (A) horizontal (with the external magnetic field **H** lying in the plane), convenient for investigations of the azimuthal behavior of FMR, and (B) vertical, which allowed a change of the polar angle of **H** between perpendicular ($\theta_H=0°$) and parallel ($\theta_H=90°$) orientations with respect to the plane of the sample. Both types of mounting were also used for temperature-dependent measurements, limited however to main crystallographic axes ($[100],[110],[\bar{1}10],[001]$).

III. RESULTS

The measured FMR spectra are shown in Figs. 3 and 4. The narrow line just below 2000 G originates from the Al_20_3:Cr marker, whose well-known paramagnetic reso-

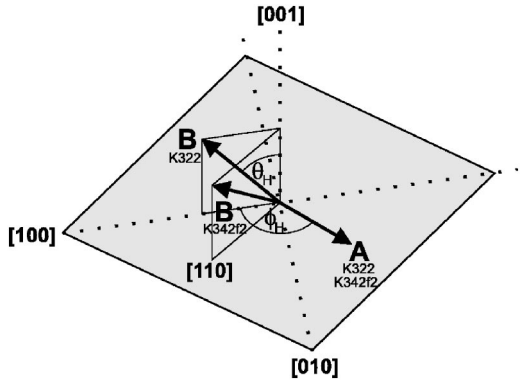

FIG. 2. The geometry of experiment. Arrows indicate the orientation of the external magnetic field vector: in position A the azimuthal angle ϕ_H was varied, B—the polar angle θ_H. Note, that polar investigations of both samples were performed in different crystallographic planes.

nance with the effective g-factor equal 3.3428 was relevant in a precise determination of the microwave frequency. Three weak lines (partially resolved quintet) in the range 2800−4000 G of Fig. 3 are the fingerprint of iron from the InP:Fe substrate.[13] They are almost invisible in Fig. 4 due to much higher intensity of the FMR signal of the K324f2 sample as compared with K322. In both cases, the angular behavior of the Fe quintet confirms the macroscopic orientation of crystallographic axes as deduced from cleaving edges of the samples.[14]

The uniform mode of FMR is represented in Figs. 3 and 4 by a distinct, relatively broad line (ΔH_{pp}=200−1000 G)

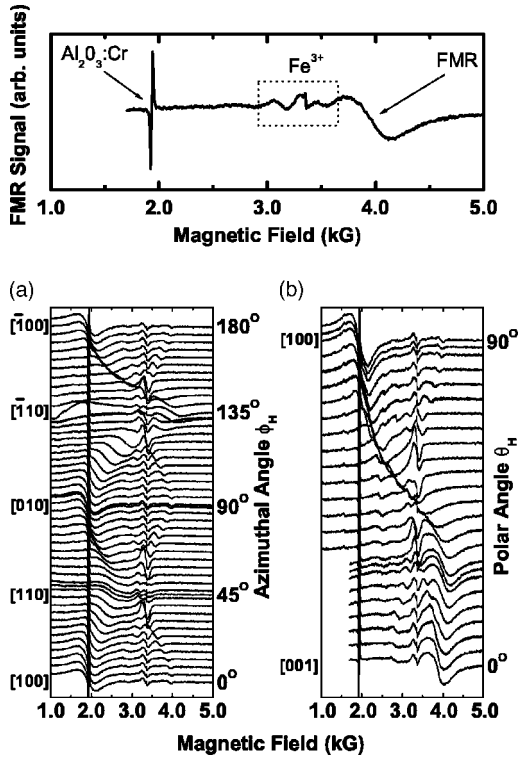

FIG. 3. As-measured FMR spectra of the K322 sample: a typical spectrum (top), in-plane (bottom, a) and out-of-plane (bottom, b) anisotropy.

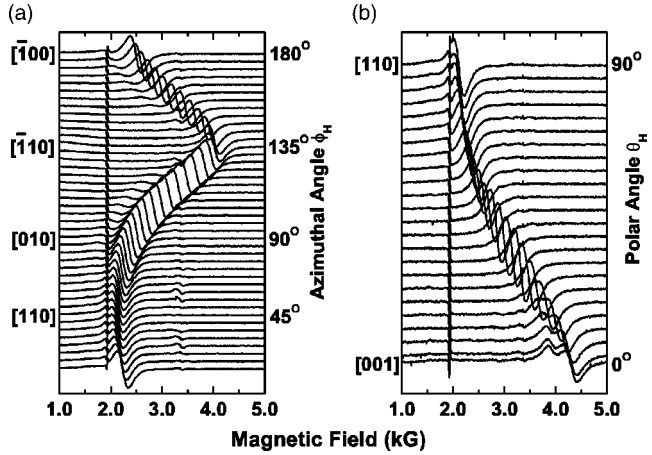

FIG. 4. As-measured FMR spectra of the K342f2 sample: in-plane (a) and out-of-plane (b) anisotropy.

with the resonance magnetic field H_{res} varying in the range of about 1800−4000 G for K322 and 2100−4300 G for K342f2. Left (a) panels indicate two alternative symmetries of the azimuthal behavior. For K322 the interplay between cubic and uniaxial anisotropy is observed, resulting in identical minima of $H_{res}(\phi_H)$ for the external field **H** around [100], [010] and $[\bar{1}00]$ directions, and in two different maxima for [110] and $[\bar{1}10]$ having resonance fields of about 2500 G and 4000 G, respectively. On the other hand, in the plane of the K342f2 sample one finds strong uniaxial anisotropy with the admixture of a cubic component occurring only in different widths of extrema of $H_{res}(\phi_H)$: the minimum for [110] and the maximum for $[\bar{1}10]$. The polar results, revealing the minima of $H_{res}(\theta_H)$ for θ_H=90°, confirm that [100] for K322 and [110] for K342f2 are the easy-axes of magnetization. In spite of the same planar position of easy-axes appearing in both samples, there is an interesting difference in the orientation of hard-axes. In Fig. 3(b) one can see that FMR line reaches its maximum resonance field for **H** tilted about 30 degrees out of the [001] direction, which is the hard-axis for a K342f2 sample. This unusual feature can be explained in a qualitative way as the interplay between cubic and uniaxial magnetocrystalline anisotropies. A more thorough discussion of all these results will be given in Sec. V on the basis of the MAE model introduced below

Note the additional lines at the low-field side of the uniform mode in Fig. 4, which cannot be ascribed to the spin-wave resonance (SWR) in the case of the 50 nm thick sample (in as-grown GaMnAs, for example, the spin-wave lines disappear for thicknesses less than ~100 nm).[15,16] Similar features were observed for metallic layers and heterostuctures. For Fe/GaAs and Fe/ZnSe films[17,18] two-line resonance spectra were observed using conventional and photothermally modulated FMR. In the case of angle-dependent FMR investigations of Fe/ZnSe, supported by SQUID data, the additional mode was attributed to a nonuniform excitation of the magnetization resulting from vertical (along direction perpendicular to the film plane) inhomogeneity of the sample.[17] Recently spin-wave resonance experiments performed for epitaxial GaMnAs revealed linear de-

pendence of SWR mode positions on the mode index.[16,19] This exception from Kittel's quadratic dispersion[20] was interpreted on the basis of the volume-inhomogeneity model proposed by Portis,[21] assuming nonuniform magnetic properties (magnetization and/or uniaxial anisotropy) along the growth direction. The origin of the gradient in the magnetic properties is still unresolved, but the speculative discussion of explanations can be found in Refs. 16 and 19.

IV. MODEL

Presented experimental data can be interpreted in the Magnetic-Anisotropy-Energy (MAE) model, already successfully used in the explanation of FMR studies of metallic ferromagnets[1] and recently applied to GaMnAs.[6] It is worthwhile to note that our approach is more general as it does not need any arbitrary assumption about the relative orientation of the magnetization **M** and the external magnetic field **H**. In Ref. 6, **M** is assumed to be parallel to **H** for high symmetry axes: [001], [110], $[\bar{1}10]$ and [100]. It will be shown that the condition $\mathbf{M}\|\mathbf{H}$ is not justified, e.g., for $\mathbf{H}\|[100]$ at a finite temperature.

For clarity of discussion we recall here the basic formulas derived by Smit and Beljers[22] from the classical equation of motion of the magnetization **M** (Laundau-Lifschitz equation):

$$\frac{d\mathbf{M}}{dt} = -\gamma \mathbf{M} \times \mathbf{H}, \tag{1}$$

where $\gamma = g\mu_B/\hbar$ is the gyromagnetic ratio. Assuming small harmonic deviations of the **M** direction from the equilibrium position and expanding free energy F of the magnetization in the external magnetic field into a Taylor series up to 2nd order terms, one gets the general formula

$$\left(\frac{\omega_{res}}{\gamma}\right)^2 = \frac{1}{M^2 \sin^2\theta_{eq}}\left(\left.\frac{\partial^2 F}{\partial \theta_M^2}\right|_{\theta_{eq},\phi_{eq}} \cdot \left.\frac{\partial^2 F}{\partial \phi_M^2}\right|_{\theta_{eq},\phi_{eq}} - \left(\left.\frac{\partial^2 F}{\partial \theta_M \partial \phi_M}\right|_{\theta_{eq},\phi_{eq}} \right)^2 \right), \tag{2}$$

where ω_{res} is the resonance frequency. The spherical coordinates θ_{eq}, ϕ_{eq} denote the equilibrium position of the magnetization, given by the minimum of F. Free energy (as a function of **M** and **H**) depends on the shape of the sample, as well as its crystallographic structure. In general there are three contributions to F: (a) Zeeman $F_{Zeeman} = -\mathbf{H}\cdot\mathbf{M}$, (b) demagnetization F_{demag}, and (c) magnetocrystalline F_{mc} energy. In the case of epitaxial layers of (001) orientation the shape contribution may be approximated by the formula describing demagnetization energy of the infinite plane:

$$F_{demag} = 2\pi M^2 \cos^2\theta_M. \tag{3}$$

The magnetocrytalline contribution to free energy F for specific crystal structures can be found in Ref. 1. In this paper the tetragonal symmetry was assumed to describe vertically distorted epitaxial samples. This choice was justified by failed attempts of the application of a MAE model with a cubic structure to the presented FMR data of InGaMnAs as well as unpublished results obtained by us for GaMnAs. Then, the magnetocrystalline energy is parametrized by three anisotropy fields $H_{2\perp}$, $H_{4\|}$, $H_{4\perp}$:

$$F_{mc} = -\frac{M}{2}\cdot\left(H_{2\perp}\cos^2\theta_M + \frac{1}{2}H_{4\perp}\cos^4\theta_M + \frac{1}{8}H_{4\|}(3+\cos(4\phi_M))\sin^4\theta_M \right), \tag{4}$$

however in order to explain in-plane anisotropy in the case of epitaxial strained sample the additional fourth term,

$$\frac{M}{4}H_{2\|}\sin(2\phi_M)\sin^2\theta_M, \tag{5}$$

needs to be considered.

The calculations were performed as follows: (a) For a certain set of anisotropy fields and an actual orientation of the external magnetic field **H**, the equilibrium position of **M** vector (angles: θ_{eq}, ϕ_{eq}) was determined by numerical minimization of free energy. Then, (b) the resonance magnetic field was derived from Eq. (2). (c) The steps (a)–(b) were repeated for different θ_H or ϕ_H values in the range of interest. (d) The predictions of the MAE model were compared with the experimental data of H_{res} and, if necessary, the anisotropy parameters were changed and the whole procedure was repeated. It should be mentioned that a fitting algorithm was prepared to compensate small deviations of the sample position from demanded horizontal or vertical orientation. The equilibrium position of the magnetization [strictly: zeros of $(\partial F/\partial\theta_M)(\theta_M,\phi_M,H_{res}(\theta_M,\phi_M))$, $(\partial F/\partial\phi_M)(\theta_M,\phi_M, H_{res}(\theta_M,\phi_M))$ corresponding to the minimum of free energy] was determined with Newton's method.

A. Anisotropy of FMR

From Eq. (2) one can derive the magnetic field of the resonance H_{res} for any orientation of **H**. As mentioned in Sec. II, our samples were investigated in two positions with respect to the external field, allowing a change of either azimuthal ϕ_H or polar θ_H angle of **H**. In Fig. 5, $H_{res}(\phi_H)$ curves are plotted for anisotropy fields listed in Table I(a). The bottom curve (#5) shows strong uniaxial anisotropy with an in-plane easy- and hard-axis of the magnetization lying along [110] and $[\bar{1}10]$, respectively. The lines #1–#4 depict a competition of two- and four-fold symmetry, with two different in-plane hard-axes [110] and $[\bar{1}10]$, perpendicular to each other and holding their directions. On the contrary, the positions of easy-axes strongly depend on MAE model parameters. With rising uniaxial field $H_{2\|}$ and diminishing cubic parameter $H_{4\|}$, they move from [100] and [010] to [110], and finally merge into a single easy-axis.

Figure 6 presents out-of-plane anisotropy curves $H_{res}(\theta_H)$ for various $H_{2\|}$, $H_{2\perp}$, $H_{4\|}$, $H_{4\perp}$ [Table I(b)]. The curve #3 corresponds to the cubic crystallographic structure, when fourth-order MAE parameters $(H_{4\|}, H_{4\perp})$ are equal and second-order $(H_{2\|}, H_{2\perp})$ vanish. There are two identical minima at equivalent directions [100] and [001], and the

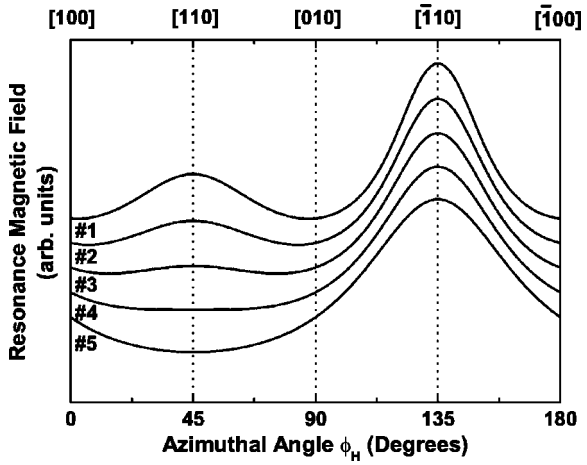

FIG. 5. In-plane anisotropy for various sets of MAE model parameters given in Table I(a).

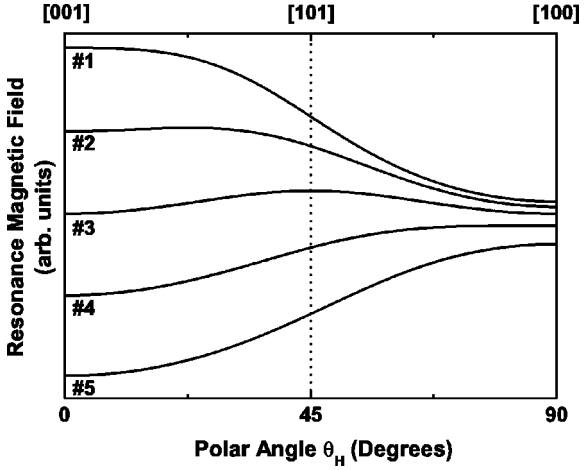

FIG. 6. Out-of-plane anisotropy for various sets of MAE model parameters given in Table I(b).

maximum for [101], according to clear, four-fold symmetry of cubic crystal. The other curves represent out-of-plane anisotropy of lower, tetragonal symmetry, e.g., for the vertically distorted sample. As reported by Liu *et al.*[6] for tetragonal GaMnAs, in the case of compressive strain in the sample plane one gets the in-plane easy-axis (here the curves #1 and #2), while for tensile strain the minimum of $H_{res}(\theta_H)$ arises at a perpendicular direction (#4 and #5). The position of the hard-axis depends on values of model parameters. When uniaxial fields $H_{2\|}$, $H_{2\perp}$ are sufficiently large the maximum of $H_{res}(\theta_H)$ reaches [100] or [001], and stays at one of these directions.

The specific theoretical curves shown in Fig. 6 result only from the magnetocrystalline part of free energy. For clarity, the contribution of demagnetization field arising from the dipole-dipole interaction of magnetic moments in a thin plane-parallel sample is not included. The shape-anisotropy

TABLE I. The anisotropy fields of the MAE model corresponding to theoretical curves presented in Figs. 5 and 6.

(a) In-plane anisotropy.

#	$H_{2\|}$ (G)	$H_{2\perp}$ (G)	$H_{4\|}$ (G)	$H_{4\perp}$ (G)[a]
1	800	−400	800	—
2	900	−200	650	—
3	1000	0	500	—
4	1100	200	350	—
5	1200	400	200	—

(b) Out-of-plane anisotropy.

#	$H_{2\|}$ (G)	$H_{2\perp}$ (G)	$H_{4\|}$ (G)	$H_{4\perp}$ (G)
1	800	−400	800	−200
2	400	−200	500	0
3	0	0	200	200
4	400	200	−100	400
5	800	400	−400	600

[a]The cubic parameter $H_{4\perp}$ does not change the shape of azimuthal anisotropy.

modifies presented curves yielding higher resonance field for **H** perpendicular to the plane (here, for **H**$\|$[001]), especially if the magnetization is relatively large, i.e., $4\pi M$ is comparable with magnetocrystalline parameters of MAE model (this is the case of the K342f2 sample, which revealed $4\pi M \approx 900$ G). In other words, due to the demagnetization field the in-plane orientation of **M** is preferred. This effect superimposes on the polar behavior of FMR originating from a given crystal structure and elevates the anisotropy curve around [001]. Therefore for samples with a tensile strain and sufficiently high magnetization the easy-axis may be shifted out of the perpendicular direction.

B. Magnetization-dependence of anisotropy

The standard approach in the explanation of temperature-dependent investigations of FMR in metallic ferromagnets is based on the assumption that magnetic anisotropy is influenced by temperature solely via deviations of the vector of local magnetization from the macroscopic orientation of **M**.[7,23] The magnitude of the local magnetic moment is regarded as independent of temperature. Zener's analysis[7] results in the following dependence of anisotropy parameters on the magnetization:

$$\kappa_l \propto \left(\frac{M(T)}{M(0)}\right)^{l(l+1)/2}, \tag{6}$$

where κ_l are the coefficients in the expansion of the magnetocrystalline part of free energy into spherical harmonics $Y_l^m(\theta_M, \phi_M)$:

$$F_{mc} = \kappa_0 Y_0^0 + \kappa_2 Y_2^0 + \kappa_4 Y_4^0 + \ldots . \tag{7}$$

There were reported several experimental results of temperature-dependent FMR investigations in bulk metallic ferromagnets confirming the above $l(l+1)/2$-power-law" (see Refs. 1, 7, and 23 and references within). However the case of epitaxial layers is more complicated due to a different temperature dependence of the anisotropy in the interior and at the frontiers of the film.[1] The unknown "bulk" and "sur-

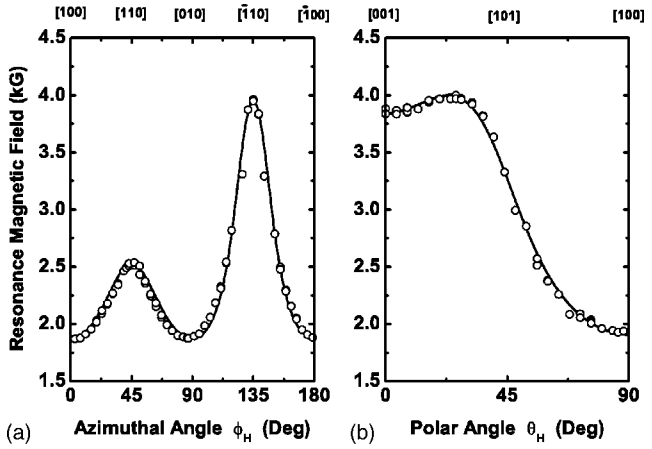

FIG. 7. Azimuthal (a) and polar (b) dependence of the resonance field of K322 sample with fitted theoretical anisotropy according to MAE model. The pairs of points appearing at certain angles are the resonance fields regarded as centers of the lines supplemented with mean values of magnetic fields corresponding to minimum and maximum of the spectra. Fitting parameters are collected in Table II.

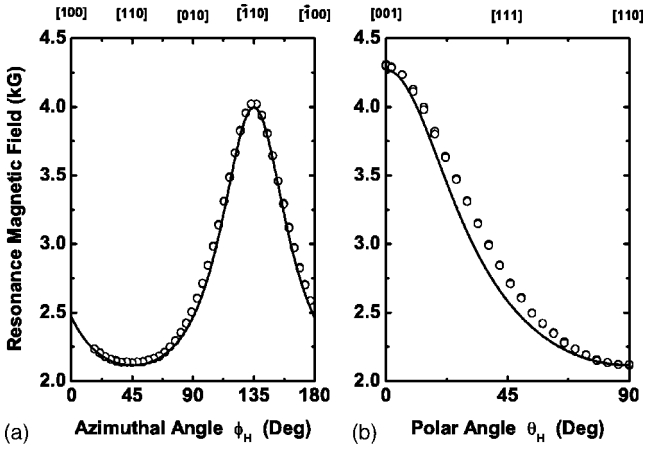

FIG. 8. Azimuthal (a) and polar (b) dependence of the resonance field of the K342f2 sample with fitted theoretical anisotropy according to the MAE model. Fitting parameters are collected in Table II.

face" contributions to the anisotropy may result in quite different power-laws than proposed by Zener. In our analysis we decided to derive the magnetization-dependent behavior of κ_l from collected experimental data, and then compare it with Zener's predictions.

The magnetocrystalline part of free energy [Eqs. (4) and (5)] can be expressed with spherical harmonics in the following way:

$$\begin{aligned} F_{mc} &= \kappa_0 Y_0^0 + \kappa_2 Y_2^0 + \kappa_{22} i(Y_2^2 - Y_2^{-2}) + \kappa_4 Y_4^0 + \kappa_{44}(Y_4^4 + Y_4^{-4}) \\ &= \frac{1}{2\sqrt{\pi}}\left(\kappa_0 - \frac{\sqrt{5}}{2}\kappa_2 + \frac{9}{8}\kappa_4\right) + \frac{3}{4\sqrt{\pi}}\left(\sqrt{5}\kappa_2 - \frac{15}{2}\kappa_4\right) \\ &\times \cos^2\theta_M - \frac{1}{2}\sqrt{\frac{15}{2\pi}}\kappa_{22}\sin(2\phi_M)\sin^2\theta_M \\ &+ \frac{105}{16\sqrt{\pi}}\kappa_4\cos^4\theta_M + \frac{3}{8}\sqrt{\frac{35}{2\pi}}\kappa_{44}\cos(4\phi_M)\sin^4\theta_M. \end{aligned} \tag{8}$$

Comparing coefficients preceding the corresponding trigonometric components of the above formula and Eqs. (4) and (5), one gets κ_l coefficients expressed as a linear combination of the experimental anisotropy parameters $K_m = MH_m/2$ $(m = 2\|, 2\perp, 4\|, 4\perp)$:

TABLE II. Anisotropy fields of the MAE model applied to investigated InGaMnAs samples.

Sample	$H_{2\|}$ (G)	$H_{2\perp}$ (G)	$H_{4\|}$ (G)	$H_{4\perp}$ (G)
K322	860	−540	910	215
K342f2	1200	370	230	−470

$$\kappa_0 = -\frac{\sqrt{\pi}}{15}(10K_{2\perp} + 6K_{4\|} + 3K_{4\perp}),$$

$$\kappa_2 = -\frac{4}{21}\sqrt{\frac{\pi}{5}}(7K_{2\perp} - 3K_{4\|} + 3K_{4\perp}),$$

$$\kappa_{22} = -\sqrt{\frac{2\pi}{15}}K_{2\|},$$

$$\kappa_4 = -\frac{2\sqrt{\pi}}{105}(3K_{4\|} + 4K_{4\perp}),$$

$$\kappa_{44} = -\frac{1}{3}\sqrt{\frac{2\pi}{35}}K_{4\|}. \tag{9}$$

The magnetization-dependent behavior of κ_l can be obtained by combining FMR results $H_m(T)$ and $M(T)$ data from SQUID magnetometry. Now, one can perform a numerical approximation of $\kappa_l(M)$ as a power function of the magnetization,

$$\kappa_l \propto \left(\frac{M(T)}{M(0)}\right)^{\alpha}. \tag{10}$$

V. DISCUSSION

Figures 7 and 8 present azimuthal and polar anisotropy of the resonance magnetic field H_{res} (as derived from FMR spectra) with fitted theoretical curves. We note that the MAE model provides a reasonable description of experimental data for both samples (fitting parameters are listed in Table II). In Fig. 7(a) one can see strong competition between four-fold symmetry typical for the zinc-blende structure and two-fold uniaxial anisotropy, occurring in inequivalent [110] and $[\bar{1}10]$ directions. The difference of resonance fields for $\phi_H = 0°$ and $\phi_H = 45°$ is about 1.5 kG, much larger than ob-

served for GaMnAs.[6] The comprehensive explanation of the braking of four-fold symmetry is still lacking, it is clear however, that layer/sublayer interface plays the most crucial role in this phenomenon. Krebs *et al.* reported similar uniaxial anisotropy for cubic α-Fe films grown on GaAs.[24] They suspect its origin in a specific topology of the bonds at layer/substrate interface, distinguishing [110] and $[\bar{1}10]$ directions. On the other hand, Sawicki *et al.* emphasize that one deals with two different frontiers of epitaxial layers, layer/sublayer and layer/vacuum, braking top/bottom symmetry of the tetragonal D_{2d} point group. Therefore one has to regard lower C_{2v} symmetry.[25]

The in-plane anisotropy of the K342f2 sample [Fig. 8(a)] is quite unusual as compared with the above discussed data of K322. One finds the uniaxial behavior of $H_{res}(\phi_H)$, with two-fold symmetry slightly disturbed by a cubic component visible especially in different widths of extrema. The strong contribution of uniaxial part to the magnetocrystalline free energy is evident in MAE model parameters: the second-order anisotropy field $H_{2\|}$ is substantially larger than $H_{4\|}$, as well as than corresponding parameters obtained for sample K322 (Table II). Although the growth conditions and the composition of manganese were nominally the same for both samples (as mentioned in Sec. II), their anisotropic properties are quite different, as was the magnetization. Considering the differences in two samples studied, one may conclude that magnetic anisotropy seems to be significantly influenced by subtle changes (beyond the control) of MBE growth conditions, e.g. manganese composition or substrate temperature. This opens an interesting possibility that ferromagnetic anisotropy properties are influenced by details of the microscopic state of the alloy, i.e., particular features of its structural disorder. For instance, one can expect a specific distribution of manganese in the host lattice in metastable InGaMnAs. Such partial ordering of Mn atoms should be very sensitive to the growth conditions. Considering this specific distribution, we do not mean Mn clusters, often opposed in the literature to a random alloy approximation, but rather, more generally, a state of microscopic order of manganese in an InGaAs lattice. Even before any bigger Mn clusters are formed that could be easily detected by microscopic means, still specific atomic correlations of Mn atoms locations in the crystal lattice sites may exist. In particular, such a correlated distribution of the impurity may exhibit anisotropic features and in such a way influence the magnetic anisotropy. A kind of partial local ordering of manganese may be also responsible for a low value of the hole concentration ratio to Mn impurity concentration, $p/[Mn]=0.03$ in K342f2,[10] similar to what was recently proposed for some other highly doped materials.[26,27] Moreover recent studies of GaMnAs by scanning tunnelling microscopy (STM) suggest deviations from random distribution of Mn in GaMnAs, on the basis of the observed STM image fluctuations.[28] The presented results may indicate limitations of generally acknowledged model of diluted ferromagnetic semiconductors, assuming the random distribution of magnetic ions. In this regard it is worth mentioning the EXAFS (extended x-ray absorption fine structure) studies of metastable InMnAs alloys.[29] They revealed an existence of local distortions of the lattice, and showed that the Mn atom surrounding has the features of both the tetragonal location in the zinc blende structure, as well as the hexagonal MnAs (NiAs prototype structure). This may be consistent with the partial ordering of Mn ions proposed here. Also RBS (Rutherford backscattering) and PIXE (particle induced x-ray emission) investigations of GaMnAs[30] revealed local lattice distortions, but on the contrary, they were interpreted (assuming the approximation of the random distribution of magnetic ions) as originating from Mn atoms in the interstitial locations.

The theoretical curves fitted to out-of-plane experimental data [Figs. 7(b) and 8(b)] resemble curves #1 and #2 presented in Fig. 6. In both epilayers the minima of $H_{res}(\theta_H)$ arise at $\theta_H=90°$ (**H** in the plane). It may originate from the shape-anisotropy of the samples as well as their tetragonal distortion emphasized already in the case of GaMnAs.[6,25] The comparison of presented magnitudes of the anisotropy in the case of InGaMnAs, with the results obtained for GaMnAs/GaAs enables the discussion of the contributions of demagnetization and distortion to the observed planar confinement of easy-axes. According to Ref. 6 and our own (unpublished) results, $Ga_{1-x}Mn_xAs$ epilayers of thickness 200–300 nm and the magnetization less than 30 emu/cm^3 revealed (at low T) the amplitude of polar anisotropy $H_{res}^{out\text{-}of\text{-}plane}-H_{res}^{in\text{-}plane}$ greater than 5000 G. In the case of our $(In_{0.53}Ga_{0.47})_{0.87}Mn_{0.13}As$ samples one deals with 5–6 times thinner films and 2–3 times larger magnetization, thus one could expect an essentially larger amplitude $H_{res}^{out\text{-}of\text{-}plane}-H_{res}^{in\text{-}plane}$, if the shape-anisotropy were more important than distortion. On the contrary, both for K322 and K342f2 samples the resonance field varies with the amplitude of about 2200 G, less than one half of the value from Fig. 5 of Ref. 6. Thus we expect the magnetocrystalline anisotropy (related to the crystal structure of the film and its distortion) plays the dominant role in our InGaMnAs epilayers and is more essential than demagnetization. It is confirmed by in-plane anisotropy $H_{res}(\phi_H)$, whose total amplitude in both compounds is comparable ($\sim$2000 G), but the uniaxial component is 3 times or more stronger in InGaMnAs than GaMnAs. Liu *et al.* reported for GaMnAs the difference of $H_{res}(\phi_H)$ for $\mathbf{H}\|[110]$ and $\mathbf{H}\|[\bar{1}10]$ about 600–700 G. Our FMR investigations of GaMnAs delivered the value of $\sim$200 G, while in the case of InGaMnAs (K322) one gets 1500 G, and the sample K342f2 revealed even stronger uniaxial anisotropy.

A type of distortion may be deduced from MAE model anisotropy fields. Liu *et al.*[6] reported, that for GaMnAs/GaAs with a growth-induced compressive strain $H_{2\perp}$ is negative, unlike for films with a tensile strain (namely GaMnAs/InGaAs), for which they got $H_{2\perp}>0$. In the case of our K322 sample we found $H_{2\perp}=-540$ G. Since the demagnetization field of K322 is relatively small ($4\pi M\approx 240$ G at $T=6$ K), the in-plane position of its easy-axis must be primarily induced by compressive strain. However, the results obtained for sample K342f2 seem to contradict the above reasoning. In this case the uniaxial parameter $H_{2\perp}$ is positive, suggesting tensile strain and the inverse symmetry of polar anisotropy with the easy-axis perpendicular to the plane. Nevertheless, Fig. 8(b) shows the minimum

of polar anisotropy at $\theta_H=90°$. It is not confusing if, instead of a simplified $H_{2\perp}<0$ condition, one uses the appropriate general constraints giving the easy-axis of magnetization lying in the plane of the sample,[1]

$$H_{2\perp}+\frac{1}{2}H_{4\perp}-\frac{1}{8}[3+\cos(4\phi_{eq})]H_{4\parallel}<4\pi M,$$

$$H_{4\perp}+\frac{1}{4}[3+\cos(4\phi_{eq})]H_{4\parallel}>0, \tag{11}$$

or

$$H_{2\perp}-\frac{1}{4}[3+\cos(4\phi_{eq})]H_{4\parallel}<4\pi M,$$

$$H_{4\perp}+\frac{1}{4}[3+\cos(4\phi_{eq})]H_{4\parallel}<0, \tag{12}$$

where ϕ_{eq} denotes the azimuthal angle of the easy-axis. Taking $\phi_{eq}=0$ for the [100] direction (easy-axis of the K322 sample), and $\phi_{eq}=\pi/4$ for [110] in the case of K342f2 ($4\pi M\approx 900$ G), one can check that anisotropy fields from Table II fulfill conditions of Eqs. (11) and (12). Note that the magnetocrystalline- and the shape-anisotropy are included in the above formulas, therefore Eqs. (11) and (12) combine the influence of the strain and demagnetization field on the orientation of an easy-axis.

In the case of K322 the maximum of $H_{res}(\theta_H)$ appears to be tilted from the [001] direction. This fact results from the competition of cubic and uniaxial components of free energy F (see Sec. IV). As mentioned above, the magnetization of this sample is small as compared with the resonance magnetic field varying in the range of about 1800−4000 G, and thus its influence (via the shape-anisotropy) on the out-of-plane behavior may be neglected. The K342f2 has much larger magnetization which, accompanied with stronger tetragonal distortion visible in the azimuthal plot of Fig. 8(a), causes the fact that there is no dip in polar anisotropy at $\theta_H=0$.

The fitting procedure we used also delivers information about the orientation of the magnetization for given **H**. In general **M** is not parallel to **H**, which is visualized in Fig. 9, where a tilt of **M** from the direction of the external magnetic field vector **H** as a function of the polar angle is plotted. The presented data concern the K342f2 sample, however the other one revealed analogous polar behavior. The magnetization is parallel to the external field in the maximum [001] and the minimum [110] of $H_{res}(\theta_H)$ (for K322 the latter is [100]); for other directions the declination from **H** is less then 15 degrees. The deviation reaches its largest value for $\theta_H<45°$. It corresponds to the asymmetry of $H_{res}(\theta_H)$ with a narrow maximum and a relatively broad minimum [Fig. 8(b)]. The positive value of the tilt means $\theta_M>\theta_H$ in the entire range of the polar angle, thus the results shown in Fig. 9 confirm in a direct way the explanation of the polar anisotropy of $Ga_{1-x}Mn_xAs$ (Ref. 6) and $(In_{0.53}Ga_{0.47})_{1-x}Mn_xAs$, suggesting that **M** deviates from **H** "seeking" the easy-axis (here [110]). Note that the sign of

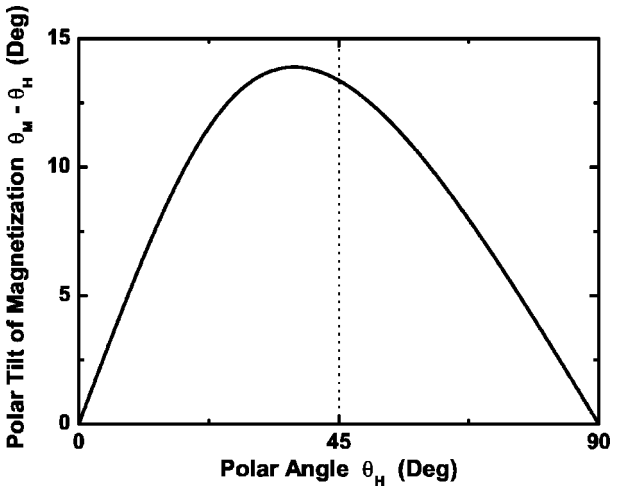

FIG. 9. Polar tilt of the magnetization $(\theta_M-\theta_H)$ of the K342f2 sample versus out-of-plane orientation of the external magnetic field.

derivative $d(\theta_M-\theta_H)/d\theta_H$ determines whether the magnetization tilts faster (positive) or slower (negative) than the external magnetic field.

Azimuthal behavior of the magnetization of the K342f2 sample (the top panel of Fig. 10) can be explained in the same way. One gets $\mathbf{M}\|\mathbf{H}$ for the maximum $[\bar{1}10]$ and the minimum [110] of $H_{res}(\phi_H)$, but the magnetization tilts faster, i.e., $d(\theta_M-\theta_H)/d\theta_H>0$, when leaves $[\bar{1}10]$ (seeking easy-axis), and slower, i.e. $d(\theta_M-\theta_H)/d\theta_H<0$, in the vicinity of [110] (trying to keep preferred, "easy" position). The case of the K322 sample (the bottom panel of Fig. 10) is more complicated. The magnetization direction coincides

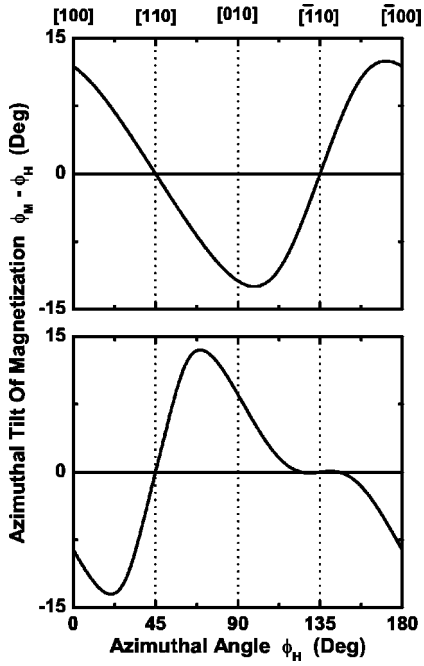

FIG. 10. Azimuthal tilt of the magnetization $(\phi_M-\phi_H)$ of K342f2 (top) and K322 (bottom) samples versus in-plane orientation of the external magnetic field.

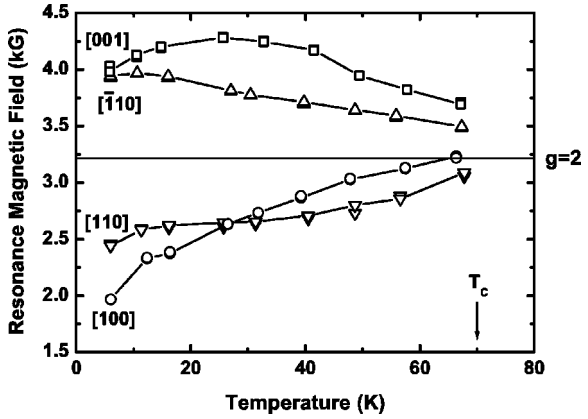

FIG. 11. Temperature dependence of the FMR resonance field of the K322 sample for the main crystallographic directions. The FMR signal disappears above $T_C \approx 70$ K.

with the external field at a maxima of $H_{res}(\phi_H)$ ([110] and [$\bar{1}$10]), showing a similar positive slope of the deviation curve as in the case $\mathbf{H}\|[\bar{1}10]$ in the top plot of Fig. 10. However for minima (here ⟨100⟩ type directions), the tilt of the magnetization is not vanishing, unlike for the K342f2 sample. The deviation is about 8°. In finite temperature the minima of azimuthal FMR anisotropy of this sample are close to ⟨100⟩ directions but do not coincide with them. Welp *et al.*[31] reported recently direct evidence of the temperature-dependent evolution of the magnetization easy-axis in compressively strained $Ga_{1-x}Mn_xAs$ epilayers. Their results obtained with a high-resolution magneto-optical imaging technique revealed a second-order magnetic transition, with the azimuthal angle of easy-axis $\phi(T)$ being the order parameter. In their studies the easy-axis is close to [100] at the lowest temperature and approaches [110] with rising T. Above the transition appearing at about $T_C/2$, the easy-axis remains at [110] direction.

Similar behavior is observed for $(In_{0.53}Ga_{0.47})_{1-x}Mn_xAs$ with interplaying uniaxial and cubic anisotropies. In Fig. 11 the resonance fields H_{res} are shown as a function of temperature for specific crystallographic directions of K322. As expected, all four sets of data approach $H_{res} \approx 3200$ G, corresponding to the effective $g=2$ of the paramagnetic resonance of a Mn ion, with temperature rising up to $T_C \approx 70$ K.[32] For temperatures below 35 K the resonance line reaches the lowest magnetic field for **H** directed between [100] and [110]. The transition is supposed to occur at about 35 K ($=T_C/2$), slightly above the intersection of data sets for [100] and [110]. According to Fig. 12 presenting the azimuthal anisotropy of K322 sample measured at 54 K ($>T_C/2$), the magnetization easy-axis holds [110] orientation. In the case of the K342f2 sample, for which uniaxial anisotropy is substantially larger, one deals with the easy-axis lying along the [110] direction already at $T=6$ K, far below $T_C/2$. Therefore no magnetic anisotropy transition is observed (see Fig. 13) and the easy-axis remains at [110] in the entire investigated temperature range. One can see that in-plane anisotropy of K322 at 54 K is similar to the low-temperature azimuthal behavior of the resonance field of the K342f2 sample pre-

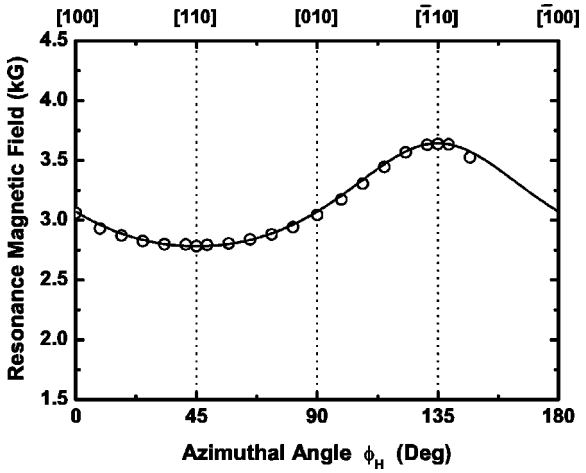

FIG. 12. In-plane anisotropy of the K322 sample for $T=54$ K. The solid line was fitted according to the MAE model with the following anisotropy fields: $H_{2\|}=570$ G, $H_{2\perp}=-20$ G, $H_{4\|}=60$ G ($H_{4\perp}$ does not influence the shape of in-plane anisotropy).

sented in Fig. 8(a). There are two main differences: Fig. 8(a) reveals essentially different widths of the extrema of $H_{res}(\phi_H)$ as compared with Fig. 12, and the magnitudes of the anisotropy are scaled with a factor of 2. Both differences find their confirmation in MAE model parameters. In the case of K322 at 54 K, one deals with a relatively larger (10–30 times) uniaxial anisotropy field $H_{2\|}$ with respect to other parameters, which in addition are close to 0. Hence the in-plane anisotropy in Fig. 12 is almost purely uniaxial and provides the symmetry of an anisotropy curve resembling $\sin(2\phi_H)$ [see in Eq. (5) the part of free energy relevant to $H_{2\|}$]. In Fig. 8(a) the anisotropy field $H_{2\|}$ is only 3–5 times larger than $H_{2\perp}$ and $H_{4\|}$, so the admixture of cubic anisotropy is clearly visible in different widths of extrema. The magnitudes of anisotropy in both discussed figures are mainly governed by the $H_{2\|}$ parameter (in the case of a dominant uniaxial component), which is indeed about 2 times larger for K342f2 at 6 K than for K322 at 54 K.

Apparently, in order to apply correctly the MAE model to describe the experiment at finite temperature, one should not assume $\mathbf{M}\|\mathbf{H}$ for ⟨100⟩ type directions, contrary to the as-

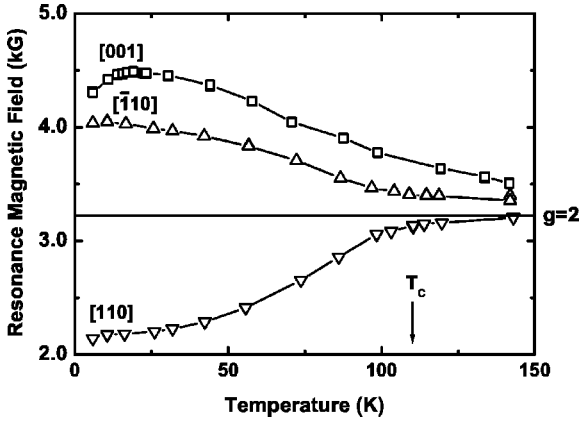

FIG. 13. Temperature dependence of the FMR resonance field of the K342f2 sample for the main crystallographic directions.

sumption of Liu *et al.*[6] At 6 K, i.e., relatively low temperature, the tilt of magnetization reaches 8–9°, about 30% of the total amplitude of $\phi_M - \phi_H$, then the incolinearity of **M** and **H** should not be neglected. In our studies, we used no arbitrary constraints about the orientation of the **M** vector with respect to both the azimuthal ϕ_M and polar θ_M angle. In addition to the results presented above, this general method confirmed that in planar (A) orientation the magnetization stays in the plane of the sample regardless of the azimuthal angle of the external magnetic field. In out-of-plane (B) orientation, by analogy, **M** remains in (010) (for the K322) or $(\bar{1}10)$ (for the K342f2) crystallographic plane.

The above discussion should be supplemented by a comparison of temperature-dependent data with paramagnetic resonance (H_{res}=3200 G depicted in Figs. 11 and 13 by a horizontal line labelled with $g=2$). The data sets corresponding to [001] and $[\bar{1}10]$ occur above 3200 G, while the ones for other main directions are shifted below paramagnetic resonance. It is in contrast to the results obtained by Liu *et al.* for GaMnAs/GaAs films, which revealed $H_{res}<3200$ G when the external magnetic field is lying in the plane of the sample, and $H_{res}>3200$ G for the perpendicular orientation of **H**. It was suggested in Ref. 6 that such behavior is typical for the epilayers under compressive strain. However, this explanation fails, if one deals with strong in-plane uniaxial anisotropy, as in the case of our $(In_{0.53}Ga_{0.47})_{0.87}Mn_{0.13}As$ films.

Note the remanent anisotropy of the K342f2 sample (Fig. 13) above its Curie temperature. This epilayer revealed very high intensity of the spectra, contrary to K322, and we suggest that the ESR signal remaining for $T \geqslant T_C$ is of paramagnetic origin, which was not possible to detect in the case of the low signal of K322. Analogous behavior was observed by Huber and Seehra in thin films of $CrBr_3$.[33] They found the exponential-like decay of $H_{res}(T)$ for perpendicular orientation of the external magnetic field **H**, and the increase for the in-plane position of the latter. These results were successfully interpreted on the basis of the temperature-dependent magnetic susceptibility tensor including the influence of the demagnetization field and possible intrinsic anisotropy of the *g*-factor. According to the formula derived by Huber and Seehra and _applied to our results, the product $(H_{res}^{[001]}H_{res}^{[110]}H_{res}^{[110]})^{1/3}$ is expected to be independent of temperature. In the case of the K342f2 sample one finds a slight decrease of this quantity, with the magnitude of about 130 G (4%) in the temperature range 110–140 K. It is hard to discuss this effect due to the lack of experimental data in the wider range of $T>T_C$. On the basis of the cited analysis of Ref. 33, for the isotropic *g*-factor [by analogy to GaMnAs and InMnAs (Ref. 32)], one can expect the same behavior of $H_{res}(T)$ for different in-plane orientations of the external magnetic field. However in Fig. 13 one finds the remanent inequivalence of [110] and $[\bar{1}10]$ directions, which may be attributed to the influence of the magnetocrystalline anisotropy, not considered by Huber and Seehra.

In order to understand temperature-dependent anisotropy, we applied Zener's analysis presented in Sec. IV B to the data shown in Fig. 11. In Fig. 14 the anisotropy coefficients κ_l for the K322 sample and power functions fitted according to Eq. (9) with the exponents listed in Table III are presented. Note the reasonable power-like behavior of κ_2, κ_{22} and κ_{44}, while the fitting procedure failed for κ_0 and κ_4. In the latter case the anisotropy coefficients κ_0 and κ_4 revealed large uncertainty (especially for $M \geqslant 14$ emu/cm^3) due to subtracting comparable values in Eq. (9). Interestingly, the exponents collected in Table III appeared essentially smaller than predicted by Zener's "$l(l+1)/2$-power-law:" $\alpha=3$ for 2nd order coefficients and $\alpha=10$ for 4th order. As mentioned in Sec. IV B, Zener's approach does not involve the possibility of different temperature-behavior of "surface" and "bulk" anisotropy. It could be estimated by separate thickness-dependent FMR investigations of InGaMnAs films of gradually diminished thickness (e.g., by etching). Moreover, we assumed that the anisotropy is influenced by temperature only via the magnetization, while one can also expect the direct dependence of κ_l on temperature due to changes of the electronic properties of the alloy. The presented problem of temperature-dependent anisotropy of InGaMnAs is still open, both in the meaning of the experiment as well as the satisfactory theoretical description.

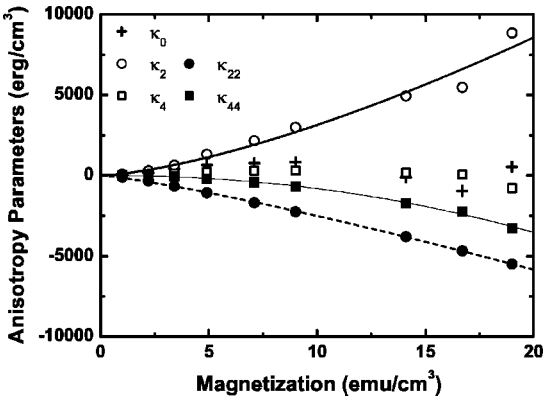

FIG. 14. Magnetization dependence of anisotropy coefficients κ_l obtained by the application of Eqs. (9) to the temperature-dependent data of Fig. 11. The lines fitted with Eq. (10) correspond to the power-like behavior of κ_2, κ_{22} and κ_{44}. The data sets of κ_0 and κ_4 do not obey the power-law given by Eq. (10) for any reasonable exponent.

VI. CONCLUSIONS

Ferromagnetic resonance was investigated in epitaxial InGaMnAs, grown lattice-matched on the InP(001) substrate in order to minimize the influence of the strain. The observed anisotropic properties of FMR find their comprehensive understanding with the Magnetic-Anisotropy-Energy model, already used for another III-V ferromagnetic semiconductor,

TABLE III. The exponents obtained by fitting the power-law given by Eq. (10) to κ_l data sets of the K322 sample depicted in Fig. 14.

	κ_0	κ_2	κ_{22}	κ_4	κ_{44}
α	-	1.4	1.2	-	2.1

namely GaMnAs. It should be emphasized that the approach presented here, based on the MAE model, provides consistent results both in the meaning of angular behavior of the resonance field and the corresponding orientation of the magnetization. The model successfully describes the anisotropy in the entire investigated temperature range, in particular the possible reorientation of the easy-axis with rising T. At higher temperatures, the FMR experiments revealed interesting power-like magnetization dependence of anisotropy coefficients, with the exponents significantly lower than predicted by standard Zener's "$l(l+1)/2$-power-law." This discrepancy was tentatively attributed to the limitations of Zener's approach, therefore the presented temperature-dependent results have to be complemented both in an experimental and a theoretical way.

For the purpose of all these experiments two samples from the series of nominally identical epilayers of ferromagnetic InGaMnAs were used. Surprisingly they revealed qualitatively different behavior: for the first sample the competition of cubic and uniaxial in-plane anisotropies was clearly observed, while for the other one strong uniaxial anisotropy was only slightly influenced by a cubic component. Since the samples were grown under the same conditions and with intentionally the same manganese composition, the differences in the magnetic anisotropy were attributed to the different microscopic state of disorder in a Mn alloy (the latter crucially depends on the growth parameters). One may expect that a relatively small change in the sample fabrication procedure results in specific correlations of the magnetic ions positions in the lattice. The origin of presented differences in disorder and their consequences were almost not discussed in the literature so far, although they influence ferromagnetic properties of III-Mn-V compounds with a comparable strength to widely reported electronic and strain-induced effects. In view of the presented results, we point out the importance of the growth procedure for a control of ferromagnetism in InGaMnAs, both in the meaning of the magnetization behavior as well as the magnetic anisotropy.

ACKNOWLEDGMENTS

This work was partially supported by The Committee for Scientific Research (Poland) under Grants No. PBZ-KBN-044/P03/2001, No. 115/E-343/SPUB-M/5.PR UE/DZ 255/2001-2003, and partially by EC under the project FENIKS (G5RD-CT-2001-00535). T.S. wishes to express special acknowledgments to Professor Hiroo Munekata of the Tokyo Institute of Technology.

*Electronic address: Konrad.Dziatkowski@fuw.edu.pl

[1] M. Farle, Rep. Prog. Phys. **61**, 755 (1998).

[2] S. A. Wolf, D. D. Awschalom, R. A. Buhrman, J. M. Daughton, S. von Molnár, M. L. Roukes, A. Y. Chtchelkanova, and D. M. Treger, Science **294**, 1488 (2001).

[3] R. Jansen, J. Phys. D **36**, R289 (2003).

[4] J. Szczytko, A. Twardowski, K. Świątek, M. Palczewska, M. Tanaka, T. Hayashi, and K. Ando, Phys. Rev. B **60**, 8304 (1999).

[5] J. Szczytko, A. Twardowski, M. Palczewska, R. Jabłoński, J. Furdyna, and H. Munekata, Phys. Rev. B **63**, 085315 (2001).

[6] X. Liu, Y. Sasaki, and J. K. Furdyna, Phys. Rev. B **67**, 205204 (2003).

[7] C. Zener, Phys. Rev. **96**, 1335 (1954).

[8] F. Matsukura, H. Ohno, and T. Dietl, in *Handbook of Magnetic Materials*, edited by K. H. J. Buschow (Elsevier, Amsterdam, 2002), Vol. 14, p. 1.

[9] H. Künzel, J. Böttcher, R. Gibis, and G. Urmann, Appl. Phys. Lett. **16**, 1347 (1992).

[10] T. Slupinski, H. Munekata, and A. Oiwa, Appl. Phys. Lett. **80**, 1592 (2002).

[11] S. Ohya, H. Kobayashi, and M. Tanaka, Appl. Phys. Lett. **83**, 2175 (2003).

[12] J. Szczytko and co-workers (Refs. 4 and 5) investigated the paramagnetic resonance of GaMnAs and InMnAs epilayers, and found the ionized Mn acceptor A^- (d^5) with a ground state spin $S=5/2$. Their results are consistent with earlier ESR studies of bulk GaAs:Mn performed by J. Schneider, U. Kaufmann, W. Wilkening, M. Baeumler, and F. Köhl, Phys. Rev. Lett. **59**, 240 (1987). Also see the results of core-level photoemission studies in GaMnAs, obtained by J. Okabayashi, A. Kimura, O. Rader, T. Mizokawa, A. Fujimori, T. Hayashi, and M. Tanaka, Phys. Rev. B **58**, R4211 (1998).

[13] According to ESR investigations of Fe^{3+} in bulk InP—performed by G. H. Stauss, J. J. Krebs, and R. L. Henry, Phys. Rev. B **16**, 974 (1977)—we deal with configuration d^5 and spin $S=5/2$. The latter results in a five-line fine structure corresponding to five possible $\Delta S=\pm 1$ transitions between $2S+1=6$ levels. See also S. G. Bishop, in *Deep Centers in Semiconductors: A State-of-the-Art Approach*, edited by S. T. Pandelides (Gordon and Breach, New York, 1986).

[14] M. Palczewska (private communication).

[15] S. T. B. Goennenwein, T. Graf, T. Wassner, M. S. Brandt, M. Stutzmann, J. B. Philipp, R. Gross, M. Krieger, K. Zürn, P. Ziemann, A. Koeder, S. Frank, W. Schoch, and A. Waag, Appl. Phys. Lett. **82**, 730 (2003).

[16] T. G. Rappoport, P. Redliński, X. Liu, G. Zaránd, J. K. Furdyna, and B. Jankó, Phys. Rev. B **69**, 125213 (2004).

[17] R. Meckenstock, D. Spoddig, K. Himmelbauer, H. Krenn, M. Doi, W. Keune, Z. Frait, and J. Pelzl, J. Magn. Magn. Mater. **240**, 410 (2002).

[18] R. Meckenstock, D. Spoddig, and J. Pelzl, J. Magn. Magn. Mater. **240**, 83 (2002).

[19] S. T. B. Goennenwein, T. Graf, T. Wassner, M. S. Brandt, M. Stutzmann, A. Koeder, S. Frank, W. Schoch, and A. Waag, J. Supercond. **16**, 75 (2003).

[20] C. Kittel, Phys. Rev. **110**, 1295 (1958).

[21] A. M. Portis, Appl. Phys. Lett. **2**, 69 (1963).

[22] J. Smit and H. G. Beljers, Philips Res. Rep. **10**, 113 (1955).

[23] For a review see H. B. Callen and E. Callen, J. Phys. Chem. Solids **27**, 1271 (1966).

[24] J. J. Krebs, B. T. Jonker, and G. A. Prinz, J. Appl. Phys. **61**, 2596

(1987).
[25] M. Sawicki, F. Matsukura, A. Idziaszek, T. Dietl, G. M. Schott, C. Ruester, G. Karczewski, G. Schmidt, and L. W. Molenkamp, arXiv: cond-mat/0212511.
[26] J. Wagner, R. C. Newman, B. R. Davidson, S. P. Westwater, T. J. Bullough, T. B. Joyce, C. D. Latham, R. Jones, and S. Öberg, Phys. Rev. Lett. **78**, 74 (1997).
[27] D. J. Chadi, P. H. Citrin, C. H. Park, D. L. Adler, M. A. Marcus, and H.-J. Gossmann, Phys. Rev. Lett. **79**, 4834 (1997).
[28] G. Mahieu, P. Condette, B. Grandidier, J. P. Nys, G. Allan, D. Stiévenard, Ph. Ebert, H. Shimizu, and M. Tanaka, Appl. Phys. Lett. **82**, 712 (2003).
[29] H. Ofuchi, T. Kubo, M. Tabuchi, Y. Takeda, F. Matsukura, S. P. Guo, A. Shen, and H. Ohno, J. Appl. Phys. **89**, 66 (2001).
[30] K. M. Yu, W. Walukiewicz, T. Wojtowicz, I. Kuryliszyn, X. Liu, Y. Sasaki, and J. K. Furdyna, Phys. Rev. B **65**, 201303(R) (2002).
[31] U. Welp, V. K. Vlasko-Vlasov, X. Liu, J. K. Furdyna, and T. Wojtowicz, Phys. Rev. Lett. **90**, 167206 (2003).
[32] J. Szczytko and co-workers (Refs. 4 and 5) reported for an epitaxially grown paramagnetic GaMnAs and InMnAs almost isotropic *g*-factor close to 2. The observed small anisotropy was attributed to a demagnetization field.
[33] D. L. Huber and M. S. Seehra, Phys. Status Solidi B **74**, 145 (1976). Also see J. Kötzler and W. Scheithe, *ibid.* **69**, 389 (1975).